**Christopher D. Davidson**
Department of Biomedical Engineering,
University of Michigan,
1420 Lurie Biomedical Engineering,
1101 Beal Avenue,
Ann Arbor, MI 48109-2110
e-mail: cddavid@umich.edu

**Danica Kristen P. Jayco**
Department of Biomedical Engineering,
University of Michigan,
1420 Lurie Biomedical Engineering,
1101 Beal Avenue,
Ann Arbor, MI 48109-2110
e-mail: danicaj@umich.edu

**William Y. Wang**
Department of Biomedical Engineering,
University of Michigan,
1420 Lurie Biomedical Engineering,
1101 Beal Avenue,
Ann Arbor, MI 48109-2110
e-mail: wangwy@umich.edu

**Ariella Shikanov**
Department of Biomedical Engineering;
Department of Macromolecular Science and Engineering,
University of Michigan,
2126 Lurie Biomedical Engineering,
1101 Beal Avenue,
Ann Arbor, MI 48109-2110
e-mail: shikanov@umich.edu

**Brendon M. Baker**
Department of Biomedical Engineering,
University of Michigan,
2174 Lurie Biomedical Engineering,
1101 Beal Avenue,
Ann Arbor, MI 48109-2110
e-mail: bambren@umich.edu

# Fiber Crimp Confers Matrix Mechanical Nonlinearity, Regulates Endothelial Cell Mechanosensing, and Promotes Microvascular Network Formation

*Mechanical interactions between cells and their surrounding extracellular matrix (ECM) guide many fundamental cell behaviors. Native connective tissue consists of highly organized, 3D networks of ECM fibers with complex, nonlinear mechanical properties. The most abundant stromal matrix component is fibrillar type I collagen, which often possesses a wavy, crimped morphology that confers strain- and load-dependent nonlinear mechanical behavior. Here, we established a new and simple method for engineering electrospun fibrous matrices composed of dextran vinyl sulfone (DexVS) with controllable crimped structure. A hydrophilic peptide was functionalized to DexVS matrices to trigger swelling of individual hydrogel fibers, resulting in crimped microstructure due to the fixed anchorage of fibers. Mechanical characterization of these matrices under tension confirmed orthogonal control over nonlinear stress–strain responses and matrix stiffness. We next examined ECM mechanosensing of individual endothelial cells (ECs) and found that fiber crimp promoted physical matrix remodeling alongside decreases in cell spreading, focal adhesion area, and nuclear localization of Yes-associated protein (YAP). These changes corresponded to an increase in migration speed, along with evidence for long-range interactions between neighboring cells in crimped matrices. Interestingly, when ECs were seeded at high density in crimped matrices, capillary-like networks rapidly assembled and contained tube-like cellular structures wrapped around bundles of synthetic matrix fibers due to increased physical reorganization of matrix fibers. Our work provides an additional level of mechanical and architectural tunability to synthetic fibrous matrices and implicates a critical role for mechanical nonlinearity in EC mechanosensing and network formation.* [DOI: 10.1115/1.4048191]

## Introduction

Native biological tissues are known to exhibit complex, nonlinear mechanical properties [1,2]. Specifically, connective tissue consists of highly organized, 3D networks of fibrillar extracellular matrix (ECM) proteins that contribute to this mechanical nonlinearity. For example, type I collagen is the most abundant stromal matrix component and exists as fibers or bundles of fibers that often possess a wavy, crimped morphology in a variety of soft tissues including tendons, ligaments, blood vessels, and the intestine [3]. External forces experienced with normal tissue function cause crimped fibers to straighten and gradually bear tensile loads. Thus, crimped fiber microstructure confers strain- and load-dependent nonlinear mechanical behaviors and contributes significantly to the overall compliance, strength, and durability of soft tissues [4,5]. Recapitulating this complex mechanical behavior is critical to engineering biomaterials for tissue engineering applications as well as better understanding cell-ECM interactions during normal and abnormal tissue function.

Electrospinning is a technique that has been extensively used to fabricate fibrous scaffolds that mimic the structure and mechanics of native tissue ECMs given its ability to generate polymeric fibers of similar length-scale as native collagen fibrils [6–8]. Additional benefits to electrospinning include its low cost, high scalability and speed of scaffold fabrication, as well as versatility in processing a wide variety of synthetic and natural polymers into fibers. By modulating attributes of the polymer solution and electrospinning process parameters, fibrous scaffolds can be fabricated with varied features that reflect the diverse landscapes of native cellular microenvironments. However, most electrospinning processes yield scaffolds containing straight fibers lacking the crimped microstructure of native collagen fibers in soft tissues. To address this limitation and generate electrospun scaffolds composed of tortuous fibers, several methods have recently been developed including electrospinning bicomponent polymeric fibers [9], air-driven electrospinning [10], magnetic-field-assisted

Manuscript received March 5, 2020; final manuscript received August 8, 2020; published online September 11, 2020. Assoc. Editor: Shannon Stott.

  

electrospinning [11], plasticizer treatment [12,13], or controlled heating above the polymer's glass transition temperature [13–18]. While these methods have successfully generated crimped fibers, resultant scaffolds lack fine control over other physical properties such as the degree of mechanical nonlinearity, matrix stiffness, and fiber density.

Additionally, the cell response to matrices composed of crimped fibers is currently not well understood. As these scaffolds have largely been developed for tendon and ligament tissue engineering applications, the cell response to external loads as a function of fiber crimp has exclusively been explored. Interestingly, these studies have shown that ligament fibroblasts and mesenchymal stem cells cultured in crimped scaffolds exhibit changes in gene expression [13,16] and cell morphology [18] under static and dynamic loading, suggesting altered mechanosensing as a function of fiber tortuosity. Recent work by our group and others support a key role for cell traction force-induced physical matrix remodeling during mechanosensing of fibrous microenvironments. Physical remodeling through fiber recruitment influences the distribution of adhesive ligand and matrix-borne forces during fundamental cell processes including cell spreading [19,20], migration [21,22], and assembly of multicellular structures [23]. However, due to the use of stiff synthetic polymeric materials ($E = 0.35$–$600$ MPa), previous fabrication methods produce matrices of crimped fibers impervious to dynamic remodeling by cell-generated forces [9–18]. We propose that nonlinear mechanics and the enhanced potential for cell force-mediated remodeling at low force regimes can regulate single cell behavior and ensuing multicellular assembly processes.

Previously, our lab has developed synthetic matrices of electrospun dextran hydrogel fibers with highly tunable architectural, mechanical, and biochemical attributes [19,24]. In separate work, we have also demonstrated control over the swelling behavior of dextran-based bulk hydrogels by modulating polymer backbone hydrophobicity via functionalization with hydrophobic methacrylates [25]. Here, we employed a similar strategy to increase hydrophilicity within the neutral polymer network of a polymer fiber in order to confer swelling behavior and crimped microstructure should the fiber be anchored at both ends. The objective of this study was to utilize this approach to examine the role of matrix fiber crimp and mechanical nonlinearity on endothelial cell (EC) behavior.

## Materials and Methods

**Reagents.** All reagents were purchased from Sigma Aldrich and used as received, unless otherwise stated.

**Cell Culture.** Human umbilical vein ECs were cultured in endothelial growth medium (EGM-2; Lonza, Basel, Switzerland) supplemented with 1% penicillin-streptomycin-fungizone (Gibco, Waltham, MA). Cells were cultured at 37 °C and 5% $CO_2$. ECs were used from passages four to eight in all experiments.

**Dextran Vinyl Sulfone Synthesis.** Dextran was reacted with divinyl sulfone following a previously described procedure [26]. Briefly, dextran (5 g) was dissolved in 250 mL of sodium hydroxide (100 mM) solution on a stir plate at 300 rpm before the addition of divinyl sulfone (12.5 mL). The reaction proceeded for 3.5 min before termination by addition of 2.5 mL hydrochloric acid (12 M). The product was dialyzed against milli-Q water for 3 days and then lyophilized. dextran vinyl sulfone (DexVS) was characterized by $^1$H NMR and a vinyl sulfone/dextran repeat unit ratio of 0.70 was determined.

**Fibrous Matrix Fabrication.** DexVS was dissolved at 0.7 g $mL^{-1}$ in a 1:1 mixture of milli-Q water and dimethylformamide with 1.2% (w/v) lithium phenyl-2,4,6-trimethylbenzoylphosphinate (LAP; Colorado Photopolymer Solutions, Boulder, CO) photoinitiator, 2.5% (v/v) methacrylated rhodamine (25 mM; Polysciences, Inc., Warrington, PA), and 5.0% (v/v) glycidyl methacrylate. Electrospinning of DexVS solution was performed at a flow rate of 0.2 mL $h^{-1}$, voltage of 7.0 kV, and gap distance of 7 cm.

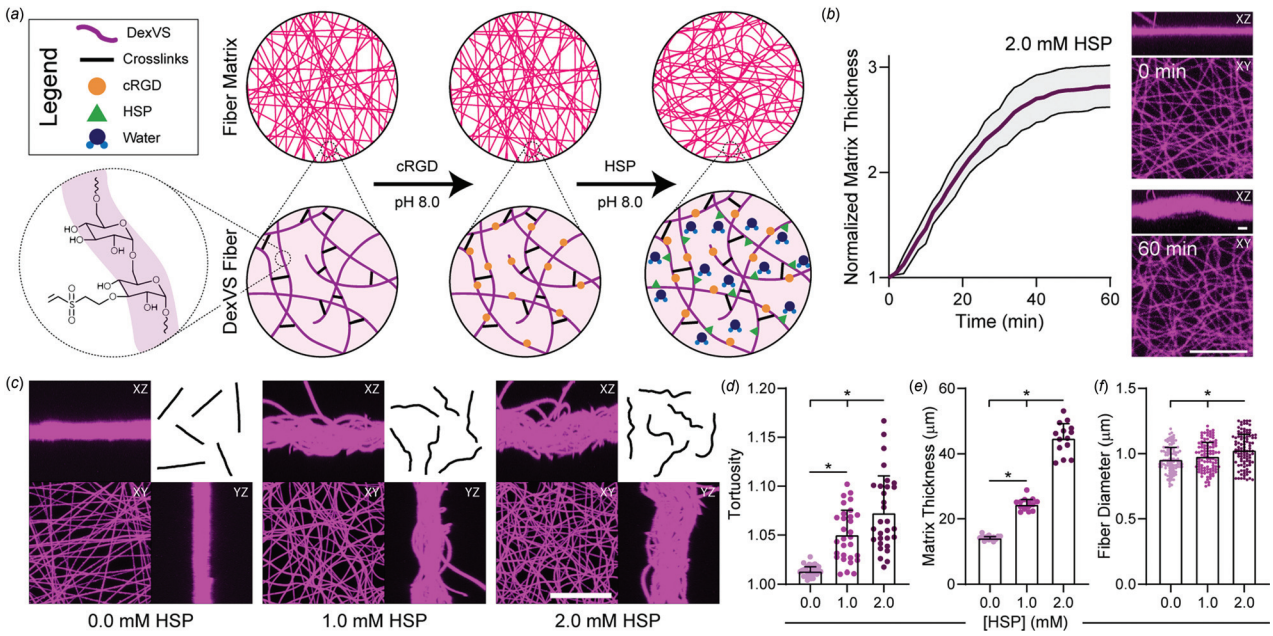


**Fig. 1 Functionalization of hydrogel fibers with HSP induces crimp in DexVS matrices. (*a*) Schematic representation of DexVS fibers with controlled adhesive ligand and crimping via functionalization with the cell adhesive peptide cRGD and hydrophilic swelling peptide (HSP, peptide sequence: CGRDGS), respectively. (*b*) Matrix thickness quantified over time immediately after adding 2.0 mM HSP ($n = 6$ matrices). (*c*) Confocal fluorescent images and orthogonal maximum intensity projections of DexVS matrices functionalized with variable HSP concentrations with representative fiber outlines. Scale bar: 50 μm. Quantification of (*d*) fiber tortuosity ($n = 30$ fibers), (*e*) matrix thickness ($n = 14$ matrices), and (*f*) fiber diameter ($n = 100$ fibers) as a function of HSP concentration. All data presented as mean ± standard deviation; *$p < 0.05$.**

After electrospinning, fibers were stabilized by primary crosslinking under UV light (100 mW $cm^{-2}$) for 120 s, hydrated in LAP solution (0.01 mg $mL^{-1}$), and then exposed again to UV light (100 mW $cm^{-2}$) for 20 s. Fibers were collected on poly(dimethylsiloxane) (PDMS; Dow Silicones Corporation, Midland, MI) arrays of circular wells produced by soft lithography as previously described [19]. Briefly, silicon wafer masters possessing SU-8 photoresist (Microchem, Westborough, MA) were produced by standard photolithography and used to generate PDMS stamps. Following silanization with trichloro(1*H*,1*H*,2*H*,2*H*-perfluorooctyl)silane, stamps were used to emboss uncured PDMS onto oxygen plasma-treated coverslips. Well arrays were methacrylated with vapor-phase silanization of 3-(trimethoxysilyl)propyl methacrylate in a vacuum oven at 60 °C for at least 6 h to promote fiber adhesion to PDMS.

**Peptide Functionalization and Seeding of Dextran Vinyl Sulfone Fibers.** DexVS fibers were first functionalized with the cell-adhesive peptide cyclo[RGDfK(C)] (cRGD; Peptides International, Louisville, KY; 100 $\mu$M) to facilitate cell attachment followed by simultaneous functionalization with the hydrophilic swelling peptide (HSP) CGRDGS (Genscript, Piscataway, NJ) and L-cysteine to induce fiber crimping. Various concentrations of HSP were coupled to control the degree of crimping, and L-cysteine was added to keep the total final peptide concentration consistent at 2 mM for all conditions. All peptides were coupled via Michael-type addition to available vinyl sulfone groups. Peptides were dissolved in milli-Q water containing HEPES (50 mM), phenol red (10 $\mu$g $mL^{-1}$), and 1 M NaOH to adjust the *p*H to 8.0. A 350 $\mu$L volume of solution was added to each substrate. cRGD and HSP/L-cysteine solutions were incubated for 30 and 45 min, respectively, at room temperature with 3× PBS rinses in between. Following peptide functionalization, substrates were rinsed 3× with PBS before cell seeding. ECs were trypsinized, centrifuged, and resuspended in 1.5% (w/v) methylcellulose supplemented EGM-2 to increase media viscosity for seeding onto suspended fibrous matrices.

**Mechanical Characterization.** To determine the tensile mechanical properties of suspended DexVS fibrous matrices, microindentation testing with a rigid cylinder was performed on a commercial CellScale Microsquisher (CellScale, Waterloo, ON, Canada). Cylinders (1 mm diameter, 0.5 mm tall) of SU8 photoresist were microfabricated and affixed to pure tungsten filaments (0.156 mm diameter, 58 mm length). Samples were indented to a depth of 350 $\mu$m at an indentation speed of 4 $\mu$m $s^{-1}$. Indenter displacement and force were converted to strain and stress, respectively. Young's modulus was calculated in both low (0.0–5.5%) and high (5.5–11.0%) strain regimes by linear fits to the stress–strain plot. Transition strain was calculated with a custom MATLAB script by finding the transition point between the toe- and linear-regions of the stress–strain data [27].

**Fluorescent Staining and Microscopy.** ECs on DexVS fibers were first fixed in 4% paraformaldehyde for 10 min at room temperature. Alternatively, to extract cytoplasmic vinculin, samples were simultaneously fixed and permeabilized in 2% paraformaldehyde in a buffer containing 1,4-piperazinediethanesulfonic acid (0.1 M), ethylene glycol-bis(2-aminoethylether)-*N*,*N*,*N*′,*N*′-tetraacetic acid (1 mM), magnesium sulfate (1 mM), poly(ethylene glycol) (4% w/v), and triton X-100 (1%) for 10 min at room temperature. To stabilize the fibers for sample processing and long-term storage, paraformaldehyde-fixed samples were crosslinked in 2 mL LAP solution (1.0% w/v) and exposed to UV light (100 mW $cm^{-2}$) for 30 s. To stain the actin cytoskeleton and nuclei, cells were permeabilized in PBS solution containing Triton X-100 (0.5% v/v), sucrose (10% w/v), and magnesium chloride (0.6% w/v), and simultaneously blocked in 1% (w/v) bovine serum albumin and stained with phalloidin and DAPI. For immunostaining, samples were permeabilized, blocked for 1 h in 1% (w/v) bovine serum albumin, and incubated with mouse monoclonal anti-vinculin antibody (1:1000, Sigma #V9264), mouse monoclonal anti-Yes-associated protein (YAP) antibody (1:1000, Santa Cruz #101199), or mouse monoclonal anti-VE-cadherin F-8 (1:1000, Santa Cruz #9989) followed by secondary antibody (1:1000, Life Technologies #A21236) for 1 h each at room temperature with 3× PBS washes in between. Fixed samples were imaged on a Zeiss LSM800 laser scanning confocal microscope (Zeiss, Oberkochen, Germany). Unless otherwise specified, images are presented as maximum intensity projections. Fluorescent images were

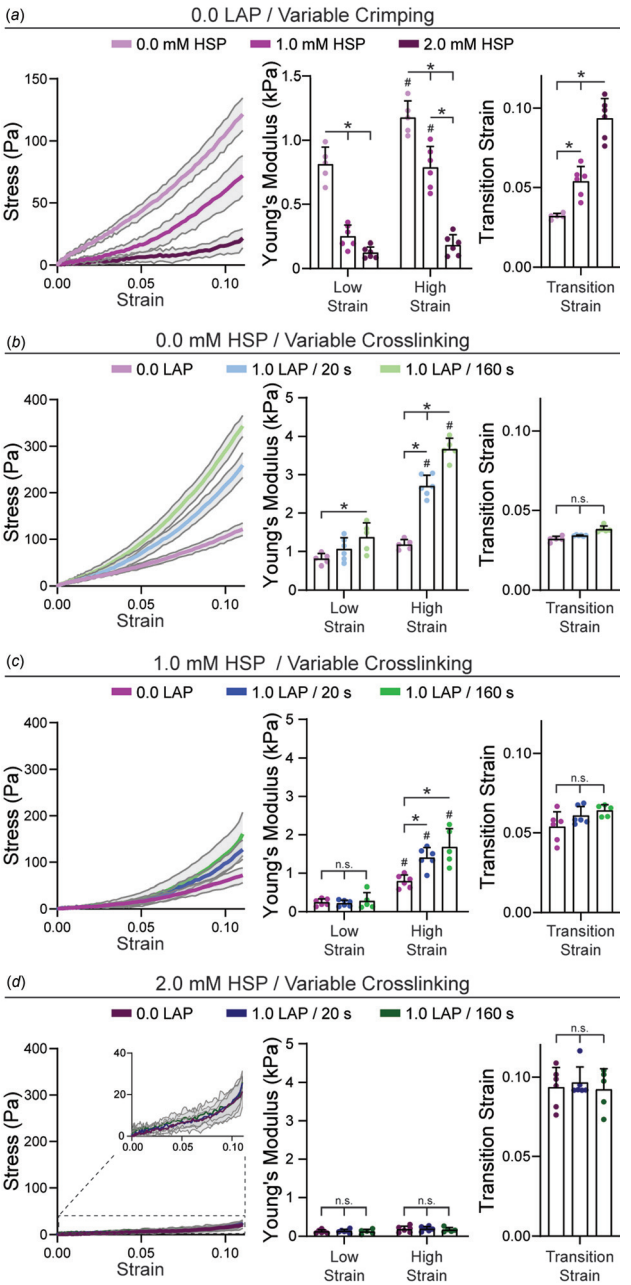


**Fig. 2 Mechanical characterization of crimped DexVS matrices. Average stress–strain curves with quantification of Young's modulus at low (0–0.055) and high (0.055–0.11) strain and transition strain for DexVS matrices with (*a*) variable HSP concentrations and no additional crosslinking, (*b*) variable crosslinking at 0.0 mM HSP, (*c*) variable crosslinking at 1.0 mM HSP, and (*d*) variable crosslinking at 2.0 mM HSP ($n = 5$–6 matrices per group). All data presented as mean ± standard deviation; *$p < 0.05$. # indicates statistical significance ($p < 0.05$) between low and high strain.**

processed and quantified via custom MATLAB scripts. Fiber recruitment was quantified by dividing the average fiber signal intensity beneath the cell body by the average fiber signal intensity outside the cell body.

**Time-Lapse Microscopy and Migration Analysis.** Time-lapse microscopy was performed on a Zeiss LSM800 laser scanning confocal microscope. Migration experiments were imaged immediately after seeding at 15 min frame intervals over 16 h. To image ECs, lentiviral transduction of lifeAct-GFP was utilized as in our previous work [28]. Immediately prior to imaging, cell nuclei were labeled with Hoechst 33342 (3 $\mu$g mL$^{-1}$) for 10 min. Following raw image export, average cell spread area was calculated for each timepoint. Additionally, cell nuclei were tracked with a custom MATLAB script predicated on the IDL particle tracking code [29]. Migration speed was calculated as total tracked distance over total tracked duration. For migration speed analysis, nuclei were only tracked between 4 and 16 h after ECs had spread.

**Statistics.** Statistical significance was determined by one-way analysis of variance with posthoc analysis (Tukey test) or Student's t-test where appropriate, with significance indicated by $p < 0.05$. Sample size is indicated within corresponding figure legends and all data are presented as mean ± standard deviation.

## Results

**Development and Mechanical Characterization of Crimped Dextran Vinyl Sulfone Fibrous Matrices.** To develop a synthetic electrospun matrix with controllable crimped microstructure, DexVS was chosen as a base polymeric material due to its amenability to electrospinning with control over matrix architecture and mechanics [24]. Matrices were fabricated by electrospinning DexVS fibers onto collection substrates such that material was suspended over an array of microfabricated PDMS wells. DexVS fibers were first functionalized with the cell-adhesive peptide cRGD via Michael-type addition to free vinyl sulfones to facilitate cell attachment, ensuring consistent cRGD concentration across all matrix conditions (Fig. 1(*a*)). We next coupled CGRDGS, a peptide containing hydrophilic arginine and glycine residues lacking cell-adhesive domains (Fig. 1(*a*)). Time-lapse confocal imaging of matrices during functionalization with this hydrophilic swelling peptide (HSP) revealed a rapid increase in fiber tortuosity as well as overall matrix thickness, presumably due to the increase in length of swelled fibers firmly anchored at well edges (Fig. 1(*b*), see Movie S1 available in the Supplemental Materials on the ASME Digital Collection.). We noted that matrices achieved a steady-state morphology 45 min after the addition of HSP, and so this duration of functionalization was utilized for all subsequent studies.

We additionally demonstrated facile control over the degree of crimping by varying the concentration of HSP coupled to DexVS matrices (Fig. 1(*c*)). Control matrices (0.0 mM HSP) possessed straight, taut fibers while increasing HSP concentration led to a stepwise increases in individual fiber tortuosity as well as overall matrix thickness (Figs. 1(*d*) and 1(*e*)). This increase in overall matrix thickness also corresponded to enhanced fiber dispersion in the *z*-direction (see Movie S2 available in the Supplemental Materials on the ASME Digital Collection.). As expected, a modest increase in fiber diameter as a function of HSP-mediated swelling was noted (control, unmodified fibers: 0.96 ± 0.10 $\mu$m versus

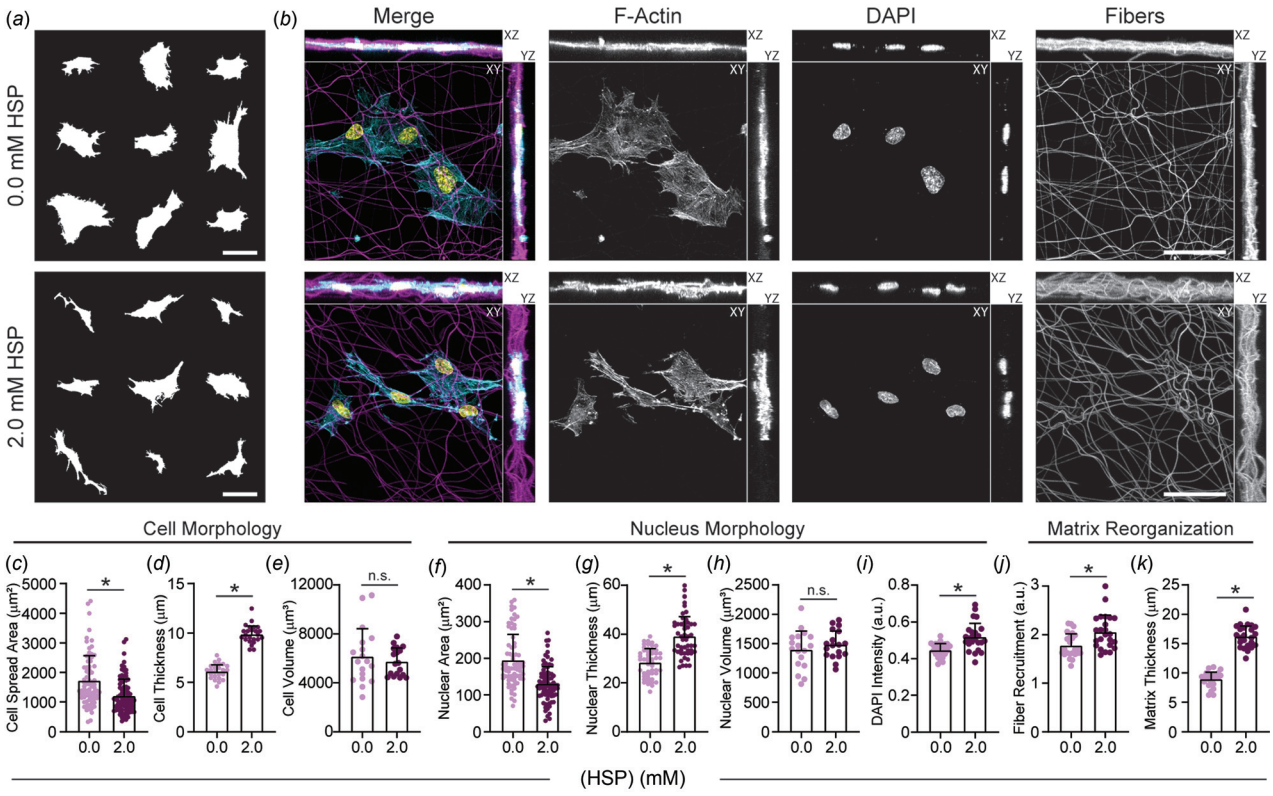


**Fig. 3 Crimped DexVS fibrous matrices regulate EC morphology and physical matrix remodeling. (*a*) Cell outlines of nine representative cells as a function of HSP concentration. (*b*) Confocal fluorescent images and orthogonal maximum intensity projections of ECs in DexVS matrices functionalized with varying HSP concentration. F-actin (cyan), DexVS fibers (magenta), nuclei (yellow). Quantification of (*c*) cell spread area ($n \geq 74$ cells), (*d*) cell thickness ($n = 24$ cells), (*e*) cell volume ($n = 18$ fields of view), (*f*) nuclear area ($n \geq 72$ nuclei), (*g*) nuclear thickness ($n = 50$ nuclei), (*h*) nuclear volume ($n = 18$ fields of view), (*i*) average DAPI intensity ($n = 24$ nuclei) (*j*) fiber recruitment ($n = 24$ fields of view), and (*k*) final matrix thickness ($n = 24$ fields of view). Scale bars: 50 $\mu$m. All data presented as mean ± standard deviation; *$p < 0.05$.**

2.0 mM HSP-functionalized fibers: 1.02 ± 0.13 μm). Although this diameter increase could impact total matrix surface area and the distribution of cell-adhesive cRGD, we anticipate these influences are negligible compared to the influence of matrix structure and mechanical behavior (Fig. 1(*f*)).

To characterize the influence of fiber crimping on matrix mechanics, the centers of suspended fibrous matrices were indented to capture stress–strain responses under tension. Similar to observations in native collagenous tissues that possess crimped architecture [3], engineered crimping of DexVS matrices led to pronounced changes in nonlinearity and a prominent toe region at low levels of strain (Fig. 2(*a*)). Noncrimped control matrices (0.0 mM HSP) possessed only a slightly nonlinear response, as seen by a modest increase in stiffness from low ($E = 812 \pm 135$ Pa) to high strain ($E = 1178 \pm 131$ Pa) regimes, potentially due to strain-dependent fiber reorientation [27,30,31]. With intermediate levels of crimping (1.0 mM HSP), we observed an increase in nonlinearity with a significant decrease in stiffness at low strain (250 ± 88 Pa) compared to control matrices. As crimped fibers would require strain-induced straightening before bearing tensile load, lower stiffness at low strain implies a diminished population of taught, load-bearing fibers. Indeed, higher strains where crimped fibers straightened and began to bear load correlated with a threefold increase in matrix stiffness (788 ± 164 Pa). At the maximum levels of crimping examined (2.0 mM HSP), the difference between stiffness at low (123 ± 45 Pa) and high (182 ± 81 Pa) strain regimes was marginal. Due to the limited testable strain range imposed by our setup and sample geometry, fibers have likely not fully straightened to bear load even at the maximum testable strain ($\varepsilon = 0.11$). We anticipate that at higher strains ($\varepsilon > 0.15$), we would observe a significant increase in stiffness for this condition. In addition to changes in Young's modulus in different strain regimes, we also noted an increase in transition strain due to a larger toe region with increasing HSP concentration (Fig. 2(*a*)).

We next orthogonally varied fiber stiffness at each level of HSP-induced crimp by crosslinking matrices for various durations (20 versus 160 s) in the presence of LAP photoinitiator after cRGD and HSP functionalization. For noncrimped control matrices, photoinitiated crosslinking led to increases in $E$ at both low and high strain regimes (Fig. 2(*b*)). With an intermediate degree of crimping, crosslinking did not influence stiffness at low strains ($\varepsilon < 0.05$), but significantly increased $E$ at higher strains (Fig. 2(*c*)). At the highest degree of crimping examined, subsequent crosslinking had no measurable effect on $E$ at either low or high strain regimes, again likely due to the lack of engagement with straightened tension-bearing fibers (Fig. 2(*d*)). Additionally, transition strain only changed as a function of HSP concentration and not as a function of photoinitiated crosslinking. Together, these results suggest that the crosslinking of single fibers only influences matrix stiffness in strain regimes where fibers are straightened and load bearing.

**Endothelial Cell Spreading and Mechanosensing in Crimped Dextran Vinyl Sulfone Matrices.** In previous work developing crimped fibrous matrices for tendon and ligament tissue engineering, cell behavior has primarily been studied in response to external static and dynamic tensile loads [13,16,18]. In addition to interpreting external mechanical cues, however, cells continuously sense and respond to passive mechanical cues from the microenvironment including matrix stiffness, topography, and dimensionality [32]. Thus, we next aimed to investigate how fiber crimp regulates EC mechanosensing and morphology. As compared to in control matrices, human umbilical vein ECs in crimped matrices exhibited a decrease in projected cell spread area (Figs. 3(*a*)–3(*c*)) and an increase in cell thickness (Figs. 3(*b*) and 3(*d*)), potentially due to the enhanced initial thickness and three dimensionality of crimped matrices (Fig. 1(*c*)). There was, however, no difference in cell volume between matrix conditions (Fig. 3(*e*)). In addition, we also noticed similar changes in nuclear morphology corresponding to differences in overall cell spreading where crimped matrices yielded nuclei with smaller projected area and increased thickness with no change in volume (Figs. 3(*f*)–3(*h*)). Interestingly, however, EC nuclei in crimped matrices had significantly increased DAPI signal intensity suggesting potential changes in chromatin density (Fig. 3(*i*)). Finally, we observed differences in physical reorganization of matrix fibers as a function of crimping. Crimped matrices exhibited increased fiber recruitment beneath the cell surface and additionally maintained increased matrix thickness as compared to control matrices (Figs. 3(*j*) and 3(*k*)). Comparing final matrix thickness to initial thickness prior to cell-seeding, though, we noted a 63% decrease in crimped matrices compared to a 34% decrease in the control. In sum, cells in crimped fiber matrices exhibited distinct morphological features and cell-ECM interactions compared to ECs cultured in noncrimped control matrices.

Given the noted changes in cell spreading with crimped matrix architecture, we next investigated the mechanosensitive proteins vinculin and YAP. Vinculin is a key force-sensitive adhesion protein and a well-established signaling molecule within focal adhesions [33,34]. In crimped matrices, we noted a decrease in both total focal adhesion area as well as single focal adhesion area as compared to control matrices (Figs. 4(*a*)–4(*c*)). Additionally, YAP is a Hippo pathway transcriptional regulator that functions as a central control point during mechanosensing [35]. In line

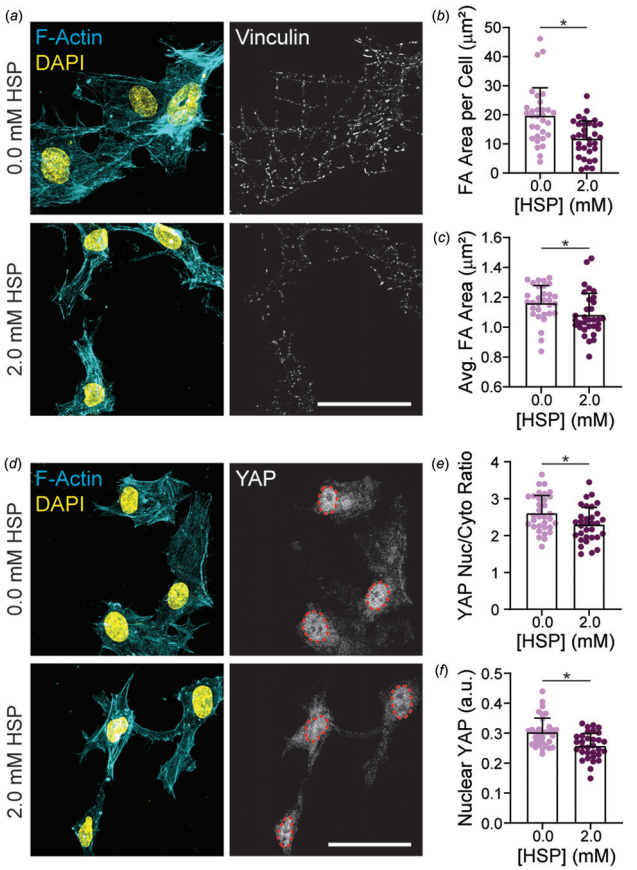


**Fig. 4 Crimped DexVS fibrous matrices regulate EC mechanosensing. Confocal fluorescent images of ECs on DexVS matrices functionalized with variable HSP concentrations and stained for (*a*) vinculin and (*d*) YAP. F-actin (cyan), nuclei (yellow). Quantification of (*b*) total focal adhesion area per cell, (*c*) average area of single focal adhesions ($n \geq 31$ cells), (*e*) YAP nuclear to cytoplasmic ratio, and (*f*) nuclear YAP intensity ($n \geq 32$ cells). Scale bars: 50 μm. All data presented as mean ± standard deviation; *$p < 0.05$.**

with previous work correlating spreading, cell adhesions, and YAP activity [36,37], we observed a lower nuclear to cytoplasmic ratio of YAP signal in cells within crimped matrices as compared to controls due to a decrease in YAP localized to the nucleus (Figs. 4(*d*)–4(f)).

**Endothelial Cell Migration and Network Formation on Crimped Dextran Vinyl Sulfone Matrices.** Examining EC phenotype at fixed timepoints is beneficial in understanding how matrix mechanics regulate cell behavior and mechanosensing. However, we also sought to examine the dynamics of cell-ECM interactions on crimped and control matrices by time-lapse live imaging (see Movies S3 and S4 available in the Supplemental Materials on the ASME Digital Collection). Over the first 4 h of culture, cells actively recruited matrix fibers without evident spreading or migration. Following this initialization period, cells began to spread and migrate in both matrix conditions (Fig. 5(*a*)). Quantifying migration speed from tracked labeled nuclei, we found that ECs migrated 13% faster on crimped matrices compared to control (Fig. 5(*b*)). Additionally, in crimped matrices we noted frequent instances of directed protrusion and migration toward neighboring cells positioned multiple cell lengths away, a phenomenon that was not observed in control matrices (Fig. 5(*c*)). Physical matrix deformations and local fiber alignment appear to generate lines of tension between cells that promoted directional cell extension, indicative of long-range mechanical communication.

Our lab and others have investigated the involvement of long-range mechanical communication in vasculogenesis, the *de novo* formation of microvascular networks [23,38]. We previously developed a model of EC network formation on suspended matrices of electrospun dextran methacrylate fibers to study in vitro vasculogenesis and discovered a critical role for physical matrix remodeling during the assembly of these complex, multicellular, capillary-like structures [23]. As crimped DexVS matrices exhibit low stiffness and increased nonlinearity at low strain regimes (Fig. 2) as well as heightened fiber recruitment by single ECs (Fig. 3), we hypothesized that crimped fibrous microstructure would also encourage EC network formation.

To investigate this, we cultured ECs at high cell density ($6 \times 10^4$ cells cm$^{-2}$) on control and crimped matrices for 5 days (Fig. 6(*a*)). While EC networks formed in both conditions with robust VE-cadherin expression at cell-cell junctions (Figs. 6(*a*) and 6(*c*)), networks on crimped matrices exhibited longer extensions between nodes while networks on control matrices had larger nodes with shorter extensions. These observations were supported by a decrease in the ratio of cell area to perimeter in crimped matrices compared to control, a previously used metric to classify network formation [23,39] (Figs. 6(*a*) and 6(*b*)). Additionally, high resolution imaging indicated increased fiber bundling and thicker cellular networks in crimped matrices, mirroring results seen earlier with single cells (Figs. 3(*j*) and 3(*k*)). Interestingly, ECs in crimped matrices wrapped around bundles of fibers, leading to the formation of tube-like structures; this phenomenon was not observed in control matrices (Figs. 6(*d*) and 6(*e*)).

## Discussion

Mimicking the architectural and mechanical properties of collagenous tissues is critical to building in vitro models for disease modeling applications and scaffolds for tissue repair. Here, we established a new approach to generating crimped electrospun synthetic polymer fibers to mimic the tortuous microstructure of fibrillar collagen in many soft tissues. By functionalizing electrospun DexVS fibrous matrices with HSP, we demonstrated control over the degree of crimping and resulting tensile nonlinearity (Figs. 1 and 2). Additionally, we utilized photoinitiated radical polymerization of DexVS fibers after functionalization with HSP to orthogonally control stiffness and fiber crimp. Noncrimped fibrous matrices exhibited relatively high Young's moduli values and more linear behavior as compared to crimped fibrous matrices possessing a low stiffness toe region followed by increased stress–strain response beyond the transition strain. Whether this degree of nonlinearity (between 5–15% strain) affects cell behavior, though, likely depends on the forces and strains that cells generate. Previous work from our lab showed cell force-induced strain up to 50% in a similar compliant fibrous matrix [22], however further analysis and quantification of cell traction forces and resulting matrix strains during dynamic physical remodeling events remains an outstanding challenge.

Regardless, we observed striking changes in cell morphology and behavior between control and crimped fibrous matrices, where fiber crimp promoted fiber recruitment and increases in cell and nuclear thickness, concurrent with decreases in cell spreading, focal adhesion area, and YAP nuclear localization (Figs. 3 and 4). These observations contrast previous results in fibrous matrices from our lab and others, where lower matrix stiffness and increased fiber recruitment correlated with increases in cell spreading and focal adhesion formation [19,20,24]. We hypothesize that this discrepancy is due to the enhanced three-dimensionality of matrices with crimped fibers (Figs. 1 and 3). Three-dimensional distribution of cell adhesions has been shown to influence cell shape, polarity, and cytoskeletal organization [40]. Forced apical-basal polarity and unrestricted planar spreading of cells plated in 2D enables distinct cytoskeletal organization compared to cells embedded in 3D ECM, which tend to assume a stellate morphology with limited polarization [41]. Further, decreases in focal adhesions and YAP nuclear localization have been noted in cells embedded within 3D hydrogels as compared to on flat, 2D surfaces [36,42,43]. In addition to the changes in dimensionality, crimped matrices exhibit a lower stress–strain response over large strain regimes which could also contribute to impaired spreading and decreased contractility.

In addition to fixed timepoint analysis, we investigated EC migratory dynamics via time-lapse microscopy. Alongside decreases in cell spreading, adhesion, and nuclear YAP localization, we observed an increase in migration speed (Fig. 5). This observation is in line with previous reports indicating that larger,

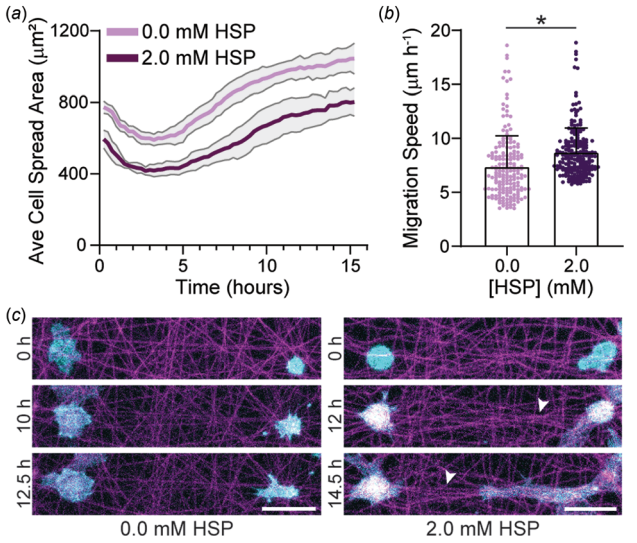


**Fig. 5 EC spreading and migration dynamics on crimped DexVS matrices. (*a*) Average cell spread area over 16 h after seeding on DexVS matrices functionalized with various HSP concentrations ($n = 6$ fields of view). (*b*) Migration speed as a function of HSP concentration ($n \geq 197$ cells). (*c*) Representative time-lapse images of lifeAct-GFP expressing ECs on DexVS matrices functionalized with 0.0 and 2.0 mM HSP. Arrows indicate matrix alignment between interacting cells. F-actin (cyan), DexVS fibers (magenta). Scale bars: 50 μm. All data presented as mean ± standard deviation; *$p < 0.05$.**

more mature adhesions imply slower adhesion turnover and lower migration speeds [44]. However, recent work from Mason et al. has linked nuclear YAP/TAZ to limiting adhesion maturation and ultimately increased migration speeds [45]. While mechanosensing is likely involved in cell migration, we anticipate other physical cues could contribute to differences in migration speed between crimped and control matrices. Specifically, the same number of fibers distributed throughout a thicker matrix implies a relative increase in porosity, which could facilitate cell migration in 3D (see Movie S2 available in the Supplemental Materials on the ASME Digital Collection.). Additionally, the low stiffness at low strains of crimped fibrous matrices enabled prominent fiber recruitment and large matrix deformations (Fig. 3), and the formation of "strap" regions of aligned fibers spanning neighboring cells. These regions of anisotropic topography, adhesive ligand distribution, and stiffness likely direct cell protrusions and subsequent migration [46] (Fig. 5). The dynamic reorganization of matrix fibers and cell-to-cell mechanical interactions in crimped matrices may also contribute to the observed increase in migration speeds. Such a result would be supported by computational modeling studies implicating nonlinear mechanics of fibrous ECM structure in the optimization of long-range mechanical communication between cells [47–49].

Together, the formation of strap regions, long-range mechanical communication, and faster cell migration could all contribute to the enhanced self-assembly of EC networks containing tube-like structures in crimped matrices compared to controls. Increased fiber recruitment with fiber crimp ultimately causes matrix densification and restriction of potential network paths of assembling cells. These restricted paths contain tensile tracks of aligned fibers that facilitate long-range force transmission to support longer cell extensions reflected by the decrease in area to perimeter ratio with fiber crimp. Additionally, densification of matrix fibers beneath extending cells may explain the appearance of tube-like EC structures (Fig. 6). Interestingly, the polarity of tubular structures formed here parallels that of previous work spatially patterning ECs in micromolded collagen gels [50]. In these studies, ECs densified and wrapped around a collagen core to form tubules, yielding structures that anastomosed with host vasculature upon implantation [51]. While the presence of synthetic DexVS fibers within these cell structures is a potential limitation, future work could utilize crimped fibers to mediate tubulogenesis followed by triggered degradation of fibers to open lumenal space.

Beyond the potential to engineer vascularized constructs, crimped synthetic fibers may also hold potential for restoring the mechanical function of dense connective fibrous tissues. One outstanding issue with the functionality of fibrous scaffolds for tissue repair is limited cell infiltration due to dense packing of fibers and subcellular pore size. Cell invasion upon implantation, however, is critical for rapid progenitor or repair cell recruitment as well as vascularization. Our results suggest fiber crimp increases matrix porosity and cell migration speed. While many methods to

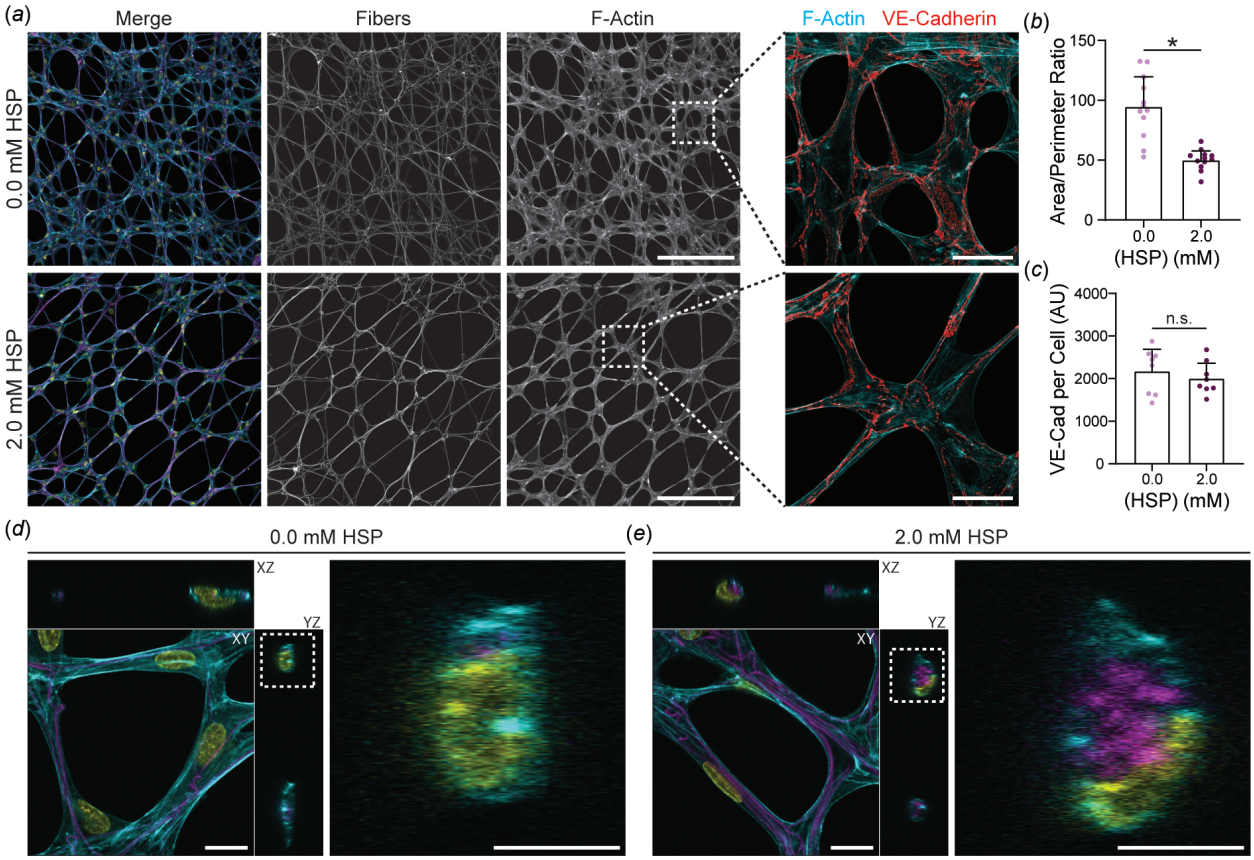


**Fig. 6 EC network formation on crimped DexVS matrices. (*a*) Confocal fluorescence images of ECs and fibers after 5 days of culture on low density DexVS matrices functionalized with variable HSP concentrations. F-actin (cyan), DexVS fibers (magenta), nuclei (yellow). Scale bar: 300 $\mu$m. Dashed boxes indicate locations of higher magnification images depicting VE-cadherin expression at cell-cell junctions. Scale bar: 50 $\mu$m. (*b*) Cell area/perimeter ratio ($n = 12$ fields of view) and (*c*) total VE-cadherin fluorescent intensity normalized to cell density ($n = 8$ fields of view) as a function of HSP concentration. Representative confocal fluorescent images and *z*-plane cross sections of tube-like structures in (*d*) control and (*e*) crimped matrix conditions. Scale bar: 10 $\mu$m. Dashed boxes indicate locations of higher magnification. Scale bar: 5 $\mu$m. All data presented as mean ± standard deviation; *$p < 0.05$.**

increase cell infiltration of fibrous scaffolds have been developed [52,53], crimped fibers could present a new strategy toward resolving this challenge.

## Conclusion

In this work, we developed a new approach to generating crimped structure in electrospun fibrous matrices by functionalizing synthetic DexVS fibers with a hydrophilic swelling peptide. This technique presents an additional level of structural and mechanical control to an already highly tunable biomaterial platform. Due to the ubiquity of fiber crimp in collagenous tissue, this unique microstructure likely has influence on cell and tissue behavior at multiple length scales. We found that matrices possessing crimped fibers led to pronounced changes in mechanical nonlinearity and regulated EC mechanosensing, migration, and network formation. The approach described here could be used in future work to better understand the influence of nonlinear ECM mechanics in healthy and abnormal tissue function and to engineer tissue constructs that more accurately recapitulate the mechanical behavior of native tissues.

## Acknowledgment

All matrix mechanical testing was carried out at the Biointerfaces Institute at the University of Michigan.

## Funding Data


- National Science Foundation Graduate Research Fellowship Program (DGE1256260; Funder ID: 10.13039/100000001).
- University of Michigan Rackham Merit Fellowship (Funder ID: 10.13039/100006801).
- NIH Pathway to Independence Award (HL124322; Funder ID: 10.13039/100000002).


## References


[1] Fung, Y. C., 1967, "Elasticity of Soft Tissues in Simple Elongation," Am. J. Physiol., **213**(6), pp. 1532–1544.

[2] Storm, C., Pastore, J. J., MacKintosh, F. C., Lubensky, T. C., and Janmey, P. A., 2005, "Nonlinear Elasticity in Biological Gels," Nature, **435**(7039), pp. 191–194.

[3] Hiltner, A., Cassidy, J. J., and Baer, E., 1985, "Mechanical Properties of Biological Polymers," Annu. Rev. Mater. Sci., **15**(1), pp. 455–482.

[4] Rigby, B. J., Hirai, N., Spikes, J. D., and Eyring, H., 1959, "The Mechanical Properties of Rat Tail Tendon," J. Gen. Physiol., **43**(2), pp. 265–283.

[5] Diamant, J., Keller, A., Baer, E., Litt, M., and Arridge, R. G., 1972, "Collagen; Ultrastructure and Its Relation to Mechanical Properties as a Function of Ageing," Proc. R. Soc. London. Ser. B. Biol. Sci., **180**(60), pp. 293–315.

[6] Mauck, R. L., Baker, B. M., Nerurkar, N. L., Burdick, J. A., Li, W.-J. J., Tuan, R. S., and Elliott, D. M., 2009, "Engineering on the Straight and Narrow: The Mechanics of Nanofibrous Assemblies for Fiber-Reinforced Tissue Regeneration," Tissue Eng. Part B Rev., **15**(2), pp. 171–193.

[7] Sill, T. J., and von Recum, H. A., 2008, "Electrospinning: Applications in Drug Delivery and Tissue Engineering," Biomaterials, **29**(13), pp. 1989–2006.

[8] Pham, Q. P., Sharma, U., and Mikos, A. G., 2006, "Electrospinning of Polymeric Nanofibers for Tissue Engineering Applications: A Review," Tissue Eng., **12**(5), pp. 1197–211.

[9] Lin, T., Wang, H., and Wang, X., 2005, "Self-Crimping Bicomponent Nanofibers Electrospun From Polyacrylonitrile and Elastomeric Polyurethane," Adv. Mater., **17**(22), pp. 2699–2703.

[10] Varesano, A., Montarsolo, A., and Tonin, C., 2007, "Crimped Polymer Nanofibres by Air-Driven Electrospinning," Eur. Polym. J., **43**(7), pp. 2792–2798.

[11] Liu, Y., Zhang, X., Xia, Y., and Yang, H., 2010, "Magnetic-Field-Assisted Electrospinning of Aligned Straight and Wavy Polymeric Nanofibers," Adv. Mater., **22**(22), pp. 2454–2457.

[12] Liu, W., Lipner, J., Moran, C. H., Feng, L., Li, X., Thomopoulos, S., and Xia, Y., 2015, "Generation of Electrospun Nanofibers With Controllable Degrees of Crimping Through a Simple, Plasticizer-Based Treatment," Adv. Mater., **27**(16), pp. 2583–2588.

[13] Chao, P.-H. G., Hsu, H. Y., and Tseng, H. Y., 2014, "Electrospun Microcrimped Fibers With Nonlinear Mechanical Properties Enhance Ligament Fibroblast Phenotype," Biofabrication, **6**(3), p. 035008.

[14] Surrao, D. C., Hayami, J. W. S., Waldman, S. D., and Amsden, B. G., 2010, "Self-Crimping, Biodegradable, Electrospun Polymer Microfibers," Biomacromolecules, **11**(12), pp. 3624–3629.

[15] Surrao, D. C., Waldman, S. D., and Amsden, B. G., 2012, "Biomimetic Poly(Lactide) Based Fibrous Scaffolds for Ligament Tissue Engineering," Acta Biomater., **8**(11), pp. 3997–4006.

[16] Surrao, D. C., Fan, J. C. Y., Waldman, S. D., and Amsden, B. G., 2012, "A Crimp-Like Microarchitecture Improves Tissue Production in Fibrous Ligament Scaffolds in Response to Mechanical Stimuli," Acta Biomater., **8**(10), pp. 3704–3713.

[17] Chen, F., Hayami, J. W. S., and Amsden, B. G., 2014, "Electrospun Poly(L-Lactide-Co-Acryloyl Carbonate) Fiber Scaffolds with a Mechanically Stable Crimp Structure for Ligament Tissue Engineering," Biomacromolecules, **15**(5), pp. 1593–1601.

[18] Szczesny, S. E., Driscoll, T. P., Tseng, H. Y., Liu, P. C., Heo, S. J., Mauck, R. L., and Chao, P. H. G., 2017, "Crimped Nanofibrous Biomaterials Mimic Microstructure and Mechanics of Native Tissue and Alter Strain Transfer to Cells," ACS Biomater. Sci. Eng., **3**(11), pp. 2869–2876.

[19] Baker, B. M., Trappmann, B., Wang, W. Y., Sakar, M. S., Kim, I. L., Shenoy, V. B., Burdick, J. A., and Chen, C. S., 2015, "Cell-Mediated Fibre Recruitment Drives Extracellular Matrix Mechanosensing in Engineered Fibrillar Microenvironments," Nat. Mater., **14**(12), pp. 1262–1268.

[20] Xie, J., Bao, M., Bruekers, M. C., and Huck, W. T. S., 2017, "Collagen Gels With Different Fibrillar Microarchitectures Elicit Different Cellular Responses," ACS Appl. Mater. Interfaces, **9**(23), pp. 19630–19637.

[21] Provenzano, P. P., Eliceiri, K. W., Campbell, J. M., Inman, D. R., White, J. G., and Keely, P. J., 2006, "Collagen Reorganization at the Tumor-Stromal Interface Facilitates Local Invasion," BMC Med., **4**(1), pp. 1–15.

[22] Wang, W. Y., Davidson, C. D., Lin, D., and Baker, B. M., 2019, "Actomyosin Contractility-Dependent Matrix Stretch and Recoil Induces Rapid Cell Migration," Nat. Commun., **10**(1), p. 1186.

[23] Davidson, C. D., Wang, W. Y., Zaimi, I., Jayco, D. K. P., and Baker, B. M., 2019, "Cell Force-Mediated Matrix Reorganization Underlies Multicellular Network Assembly," Sci. Rep., **9**(1), p. 12.

[24] Davidson, C. D., Jayco, D. K. P., Matera, D. L., DePalma, S. J., Hiraki, H. L., Wang, W. Y., and Baker, B. M., 2020, "Myofibroblast Activation in Synthetic Fibrous Matrices Composed of Dextran Vinyl Sulfone," Acta Biomater., **105**, pp. 78–86.

[25] Trappmann, B., Baker, B. M., Polacheck, W. J., Choi, C. K., Burdick, J. A., and Chen, C. S., 2017, "Matrix Degradability Controls Multicellularity of 3D Cell Migration," Nat. Commun., **8**(1), pp. 1–8.

[26] Yu, Y., and Chau, Y., 2012, "One-Step 'Click' Method for Generating Vinyl Sulfone Groups on Hydroxyl-Containing Water-Soluble Polymers," Biomacromolecules, **13**(3), pp. 937–942.

[27] Lake, S. P., Miller, K. S., Elliott, D. M., and Soslowsky, L. J., 2009, "Effect of Fiber Distribution and Realignment on the Nonlinear and Inhomogeneous Mechanical Properties of Human Supraspinatus Tendon Under Longitudinal Tensile Loading," J. Orthop. Res., **27**(12), pp. 1596–1602.

[28] Wang, W. Y., Lin, D., Jarman, E. H., Polacheck, W. J., and Baker, B. M., 2019, "Functional Angiogenesis Requires Microenvironmental Cues Balancing Endothelial Cell Migration and Proliferation," Lab Chip, **20**(6), pp. 1153–1166.

[29] Crocker, J. C., and Grier, D. G., 1996, "Methods of Digital Video Microscopy for Colloidal Studies," J. Colloid Interface Sci., **179**(1), pp. 298–310.

[30] Abhilash, A. S., Baker, B. M., Trappmann, B., Chen, C. S., and Shenoy, V. B., 2014, "Remodeling of Fibrous Extracellular Matrices by Contractile Cells: Predictions From Discrete Fiber Network Simulations," Biophys. J., **107**(8), pp. 1829–1840.

[31] Lynch, H. A., Johannessen, W., Wu, J. P., Jawa, A., and Elliott, D. M., 2003, "Effect of Fiber Orientation and Strain Rate on the Nonlinear Uniaxial Tensile Material Properties of Tendon," ASME J. Biomech. Eng., **125**(5), pp. 726–731.

[32] Ricca, B. L., Venugopalan, G., and Fletcher, D. A., 2013, "To Pull or Be Pulled: Parsing the Multiple Modes of Mechanotransduction," Curr. Opin. Cell Biol., **25**(5), pp. 558–564.

[33] Kanchanawong, P., Shtengel, G., Pasapera, A. M., Ramko, E. B., Davidson, M. W., Hess, H. F., and Waterman, C. M., 2010, "Nanoscale Architecture of Integrin-Based Cell Adhesions," Nature, **468**(7323), pp. 580–584.

[34] Grashoff, C., Hoffman, B. D., Brenner, M. D., Zhou, R., Parsons, M., Yang, M. T., McLean, M. A., Sligar, S. G., Chen, C. S., Ha, T., and Schwartz, M. A., 2010, "Measuring Mechanical Tension Across Vinculin Reveals Regulation of Focal Adhesion Dynamics," Nature, **466**(7303), pp. 263–266.

[35] Dupont, S., Morsut, L., Aragona, M., Enzo, E., Giulitti, S., Cordenonsi, M., Zanconato, F., Le Digabel, J., Forcato, M., Bicciato, S., Elvassore, N., and Piccolo, S., 2011, "Role of Yap/TAZ in Mechanotransduction," Nature, **474**(7350), pp. 179–184.

[36] Caliari, S. R., Vega, S. L., Kwon, M., Soulas, E. M., and Burdick, J. A., 2016, "Dimensionality and Spreading Influence MSC Yap/TAZ Signaling in Hydrogel Environments," Biomaterials, **103**, pp. 314–323.

[37] Nardone, G., Oliver-De La Cruz, J., Vrbsky, J., Martini, C., Pribyl, J., Skládal, P., Pešl, M., Caluori, G., Pagliari, S., Martino, F., Maceckova, Z., Hajduch, M., Sanz-Garcia, A., Pugno, N. M., Stokin, G. B., and Forte, G., 2017, "YAP Regulates Cell Mechanics by Controlling Focal Adhesion Assembly," Nat. Commun., **8**(1), pp. 1–13.

[38] Sapir, L., and Tzlil, S., 2017, "Talking Over the Extracellular Matrix: How Do Cells Communicate Mechanically?," Semin. Cell Dev. Biol., **71**, pp. 99–105.

[39] Califano, J. P., and Reinhart-King, C. A., 2008, "A Balance of Substrate Mechanics and Matrix Chemistry Regulates Endothelial Cell Network Assembly," Cell. Mol. Bioeng., **1**(2–3), pp. 122–132.

[40] Baker, B. M., and Chen, C. S., 2012, "Deconstructing the Third Dimension: How 3D Culture Microenvironments Alter Cellular Cues," J. Cell Sci., **125**(13), pp. 3015–3024.
[41] Hakkinen, K. M., Harunaga, J. S., Doyle, A. D., and Yamada, K. M., 2011, "Direct Comparisons of the Morphology, Migration, Cell Adhesions, and Actin Cytoskeleton of Fibroblasts in Four Different Three-Dimensional Extracellular Matrices," Tissue Eng. Part A, **17**(5–6), pp. 713–724.
[42] Doyle, A. D., and Yamada, K. M., 2016, "Mechanosensing Via Cell-Matrix Adhesions in 3D Microenvironments," Exp. Cell Res., **343**(1), pp. 60–66.
[43] Lee, J. Y., Chang, J. K. J., Dominguez, A. A., Lee, H., Nam, S., Chang, J. K. J., Varma, S., Qi, L. S., West, R. B., and Chaudhuri, O., 2019, "Yap-Independent Mechanotransduction Drives Breast Cancer Progression," Nat. Commun., **10**(1), p. 1848.
[44] Peyton, S. R., and Putnam, A. J., 2005, "Extracellular Matrix Rigidity Governs Smooth Muscle Cell Motility in a Biphasic Fashion," J. Cell. Physiol., **204**(1), pp. 198–209.
[45] Mason, D. E., Collins, J. M., Dawahare, J. H., Nguyen, T. D., Lin, Y., Voytik-Harbin, S. L., Zorlutuna, P., Yoder, M. C., and Boerckel, J. D., 2019, "Yap and TAZ Limit Cytoskeletal and Focal Adhesion Maturation to Enable Persistent Cell Motility," J. Cell Biol., **218**(4), pp. 1369–1389.
[46] Wang, W. Y., Pearson, A. T., Kutys, M. L., Choi, C. K., Wozniak, M. A., Baker, B. M., and Chen, C. S., 2018, "Extracellular Matrix Alignment Dictates the Organization of Focal Adhesions and Directs Uniaxial Cell Migration," APL Bioeng., **2**(4), p. 046107.
[47] Wang, H., Abhilash, A. S., Chen, C. S., Wells, R. G., and Shenoy, V. B., 2014, "Long-Range Force Transmission in Fibrous Matrices Enabled by Tension-Driven Alignment of Fibers," Biophys. J., **107**(11), pp. 2592–2603.
[48] Ma, X., Schickel, M. E., Stevenson, M. D., Sarang-Sieminski, A. L., Gooch, K. J., Ghadiali, S. N., and Hart, R. T., 2013, "Fibers in the Extracellular Matrix Enable Long-Range Stress Transmission Between Cells," Biophys. J., **104**(7), pp. 1410–1418.
[49] Sopher, R. S., Tokash, H., Natan, S., Sharabi, M., Shelah, O., Tchaicheeyan, O., and Lesman, A., 2018, "Nonlinear Elasticity of the ECM Fibers Facilitates Efficient Intercellular Communication," Biophys. J., **115**(7), pp. 1357–1370.
[50] Raghavan, S., Nelson, C. M., Baranski, J. D., Lim, E., and Chen, C. S., 2010, "Geometrically Controlled Endothelial Tubulogenesis in Micropatterned Gels," Tissue Eng. Part A, **16**(7), pp. 2255–2263.
[51] Baranski, J. D., Chaturvedi, R. R., Stevens, K. R., Eyckmans, J., Carvalho, B., Solorzano, R. D., Yang, M. T., Miller, J. S., Bhatia, S. N., and Chen, C. S., 2013, "Geometric Control of Vascular Networks to Enhance Engineered Tissue Integration and Function," Proc. Natl. Acad. Sci., **110**(19), pp. 7586–7591.
[52] Baker, B. M., Gee, A. O., Metter, R. B., Nathan, A. S., Marklein, R. A., Burdick, J. A., and Mauck, R. L., 2008, "The Potential to Improve Cell Infiltration in Composite Fiber-Aligned Electrospun Scaffolds by the Selective Removal of Sacrificial Fibers," Biomaterials, **29**(15), pp. 2348–2358.
[53] Wu, J., and Hong, Y., 2016, "Enhancing Cell Infiltration of Electrospun Fibrous Scaffolds in Tissue Regeneration," Bioact. Mater., **1**(1), pp. 56–64.